Hindawi Publishing Corporation
Journal of Nanomaterials
Volume 2008, Article ID 858235, 8 pages
doi:10.1155/2008/858235

Research Article

Mesoscale Compositionally Modulated Nanocrystalline Ni-Fe Electrodeposits for Nanopatterning Applications

P. Egberts and G. D. Hibbard

Department of Materials Science and Engineering, University of Toronto, 184 College Street, Toronto, ON, Canada M5S 3E4

Correspondence should be addressed to G. D. Hibbard, glenn.hibbard@utoronto.ca

Received 9 February 2008; Accepted 18 May 2008

Recommended by Bohua Sun

A considerable range of surface nanostructures can be fabricated by the selective dissolution of elements or phases from metallic alloys. Selectively etched electrodeposited multilayers may find useful application in optoelectronic and MEMS devices. One issue with electrodeposited multilayers is that the fine-scale multilayer structure can often exhibit significant waviness if the band layer spacing is on the same order of magnitude as the grain size. In the present study, the mean grain size was reduced to below 10 nm in a compositionally modulated Ni-Fe alloy. Preferential etching on the electroform cross-section resulted in highly uniform and directional surface channels. The evolution of this nanopatterned surface morphology was characterized by atomic force microscopy and directional roughness parameters were obtained.

1. INTRODUCTION

Selective dissolution in which one element or phase is preferentially removed from an alloy can be used to create a considerable range of functional surface nanostructures [1–5]. For example, electrochemical dealloying of single-phase Au-Ag solid solutions can be used to create nanoporous surface morphologies [e.g., [1, 2]]. In the case of multiphase alloys, Re nanowire assemblies have been produced by the selective etching of the NiAl-Re eutectic [3] and gas permeable nanoporous superalloy membranes have been fabricated by preferential dissolution of the γ' phase in a Ni-based superalloy forming several hundred nm wide interconnected channels [4, 5].

The selective etching of multilayers can also be used to generate μm- and nm-scale surface morphologies. Relatively large scale dissolution of multilayered electrodeposits can be used to produce three-dimensional components in micro-electromechanical systems (MEMSs), such as microgears [6] and microradiators [7]. Smaller scale dissolution can be used to generate nanopatterned surface morphologies for nanoimprint lithography applications, for example, opto-electronic devices [8, 9]. NiCu/Cu [8], NiFeCu/Cu [8], and CoNiFeCu/Cu [9] multilayers have been electrodeposited having layer thicknesses on the order of ~100 to 1000 nm and selectively etched to produce periodic nanopatterned surfaces. In one study, a nanoimprint master stamp was created which was used to transfer the surface pattern to a polymeric resin, successfully replicating the structure of the nanomould [8]. However, in certain cases, the uniformity of the structure can be significantly disturbed by multilayer waviness, a phenomenon that was attributed to the grain structure being on a comparable scale to the individual layer thicknesses [8, 9].

One way to circumvent this issue may be to electrodeposit a compositionally modulated material in which the grain size is much finer than the individual layer thicknesses. Electrodeposited nanocrystalline materials, in which the grain size is less than 100 nm, have the additional advantage of enhanced mechanical properties, such as significantly increased hardness and yield strength compared to conventional polycrystalline materials [e.g., [10, 11]]. Furthermore, nanocrystalline electrodeposits are particularly attractive for MEMS applications because the ultrafine and equiaxed grain structure results in a large number of grain boundaries contained in even the smallest feature of a microscale device [12]. Ultrafine periodic compositional modulations have recently been identified in nanocrystalline Ni-Fe alloys [13].

This study uses selective dissolution of Ni-Fe electrodeposits having a mean grain size of less than 10 nm to create periodic and regular nanopatterned surfaces.

2. EXPERIMENTAL

A free-standing nanocrystalline Ni-53%Fe electrodeposit was obtained from Integran Technologies Inc. of Toronto, Canada. Grain size reduction to the nm-scale can be achieved by controlling the electrodeposition parameters and bath chemistry such that the nucleation of new grains is favored over the growth of existing grains [14, 15]. The sample used in the present study was produced from an aqueous solution using an electrodeposition process similar to the one reported by Cheung et al. [16]. It was plated on a 150 mm × 150 mm Ti cathode to a thickness of ∼0.5 mm and mechanically stripped from the substrate. The alloy (Ni and Fe) and impurity (O and H) compositional modulations self-assembled during deposition and have been attributed to periodic fluctuations in pH at the cathode surface [13].

The overall Ni-Fe alloy composition was measured by energy dispersive X-ray spectroscopy (EDS) in a scanning electron microscope (SEM). The nanostructure of the electrodeposit was characterized by transmission electron microscopy (TEM). Samples were thinned to electron transparency by jet-electropolishing in a 10% perchloric acid, 15% acetic acid, and 75% methanol solution at −30°C with an applied voltage of 10 V. The nanopatterned surface morphologies were characterized by SEM and atomic force microscopy (AFM). Coupons were mounted in cross-section and prepared by mechanical grinding and polishing to obtain a mirror finish. Samples were etched in a 50% acetic acid and 50% nitric acid solution for times ranging from 10 seconds to 160 seconds. Constant deflection mode was used in the AFM and five scans (15 μm × 15 μm scan area) were obtained for each surface condition. Profile plots across the banded multilayers were obtained by averaging the AFM data files and were used to measure band spacing and height.

3. RESULTS AND DISCUSSION

TEM characterization showed a uniform and equiaxed nanostructure throughout the electron transparent region of the foil. Figure 1 presents typical bright field and dark field TEM images and selected area electron diffraction (SAED) pattern. The SAED pattern exhibited only the γ phase (FCC), which is consistent with previous studies of electrodeposited nanocrystalline Ni-Fe of similar concentration [e.g., [11, 16–18]]. The mean grain size was measured from dark field TEM micrographs. The grain size distribution of the Ni-53%Fe electrodeposit is presented in Figure 2. Over the approximately 550 grains measured, the sizes ranged from <5 nm to ∼20 nm, with a mean of 9 nm and a standard deviation of 4 nm; the grain size distribution followed a lognormal distribution (with μ = 8.3 nm and σ = 0.46 nm), which is typical of nanocrystalline Ni-based electrodeposits [e.g., [11, 16–18]].

At lower magnifications, the effect of compositional modulations in the electrodeposit could be seen through periodic changes in the TEM foil thickness, Figure 3. EDS line-scan characterization in a scanning transmission electron microscope (STEM) showed significant variation in the iron and nickel X-ray intensity, where dark (thicker) bands had a higher iron concentration than the lighter (thinner) bands [13]. Time-of-flight secondary ion mass spectrometry (TOF-SIMS) characterization on a polished cross-section from the same electrodeposit showed periodic contrast in the oxygen and hydrogen signals; this was interpreted in terms of periodic codeposition of nickel hydroxides [13]. The

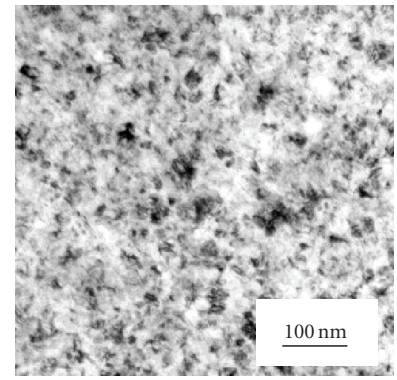

(a)

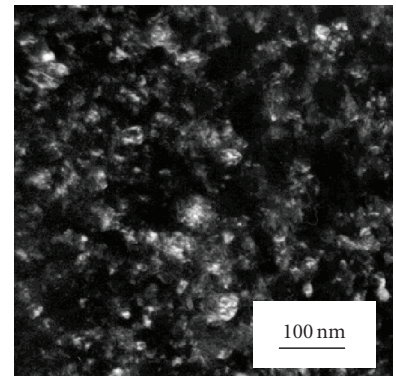

(b)

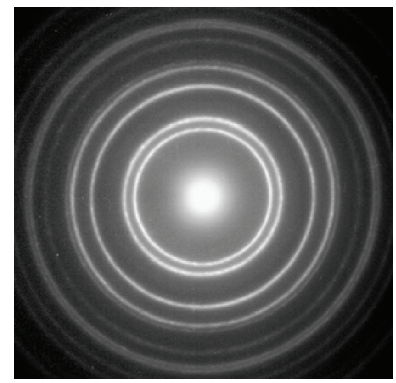

(c)

Figure 1: TEM characterization of nanocrystalline Ni-Fe electrodeposit showing bright field (a) and dark field (b) images and selected area electron diffraction pattern (c).

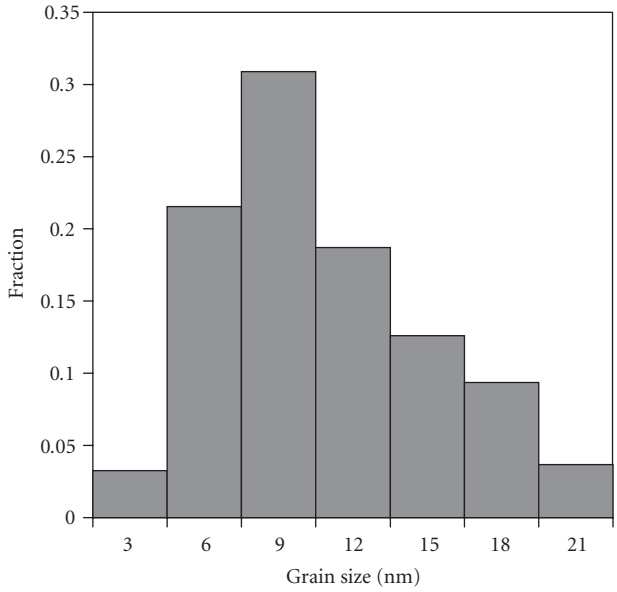

Figure 2: Grain size distribution of the nanocrystalline Ni-Fe electrodeposit.

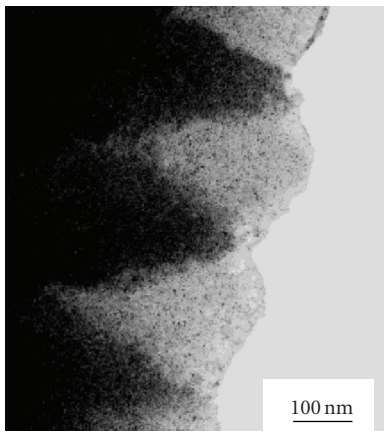

Figure 3: Low magnification plan view TEM bright field image showing thickness contrast across the compositionally modulated bands.

effect of these alloy and impurity compositional modulations could be seen in polished and etched cross-sections of the Ni-Fe electrodeposit, Figure 4. A pattern of straight recessed channels (average spacing of 650 nm) that were continuous along the cross-section and aligned perpendicular to the growth direction could be seen throughout the deposit. These bands were remarkably straight and did not exhibit the waviness that has been seen in previous studies [8, 9]. In the present case, the band morphology is decoupled from the grain size; at 9 nm (Figure 2) the mean grain size is nearly two orders of magnitude smaller than the average band spacing of ~650 nm (Figure 4). This scaling difference should have the effect of largely eliminating any potential crystallographic orientation dependence on the dissolution kinetics, promoting ultrafine etchability.

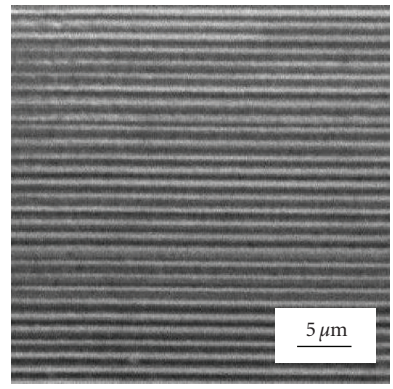

Figure 4: Typical SEM image of a polished and etched cross-section illustrating the channel morphology.

Development of the selectively etched channels was investigated by tracking the surface morphology for etching times ranging from 5 to 160 seconds. Figure 5 presents AFM profile plots recorded after 5 seconds, 10 seconds, 20 seconds, 40 seconds, 80 seconds, and 160 seconds of immersion in the 50% H_3NO_3-50% CH_3COOH etching solution. There is little apparent order to the AFM surface plot for the shortest etching time of 5 seconds and the maximum band depth (i.e., the largest difference between adjacent peaks and valley) is only ~50 nm. By 10 seconds of etching, certain bands have begun to etch deeply, some down to more than ~200 nm, but most etched channels are quite shallow. The most regular structure is observed after 40 seconds of etching, where the average channel depth is ~120 nm. The deepest channels (~500 nm) were observed in the 80-second-etched sample. Beyond this time, the maximum relative channel depth decreased and most channels were relatively shallow, on the order of ~150 nm.

The one-dimensional periodic surface morphology was quantified from profile plots in which the average height along the bands was plotted as a function of position across the bands, typical examples are shown for each etching time in Figure 6. Band spacing and band depth were measured by quantifying the distribution of local maxima and minima on the surface profile plots. Individual bands were identified by a change in curvature at a local maxima or minima, corresponding to a height change of approximately 5 nm. Band spacing was defined as the distance between adjacent maxima and minima and band height was defined as the change in height between adjacent maxima/minima pairs.

Band height and band spacing are plotted as a function of etching time in Figure 7. The increase in band height is approximately linear for etching times between 5 seconds and 80 seconds, from which a differential etching rate of 3.2 ± 0.1 nm/s was determined, that is, the difference in rate of material loss for most active versus least active regions of the bands (Figure 7(a)). The plot of band spacing as a function of etching time (Figure 7(b)) is somewhat more complex. There is initially a decrease in effective band spacing from 5 seconds to 10 seconds, which occurs during the period when preferential band etching is becoming activated. From

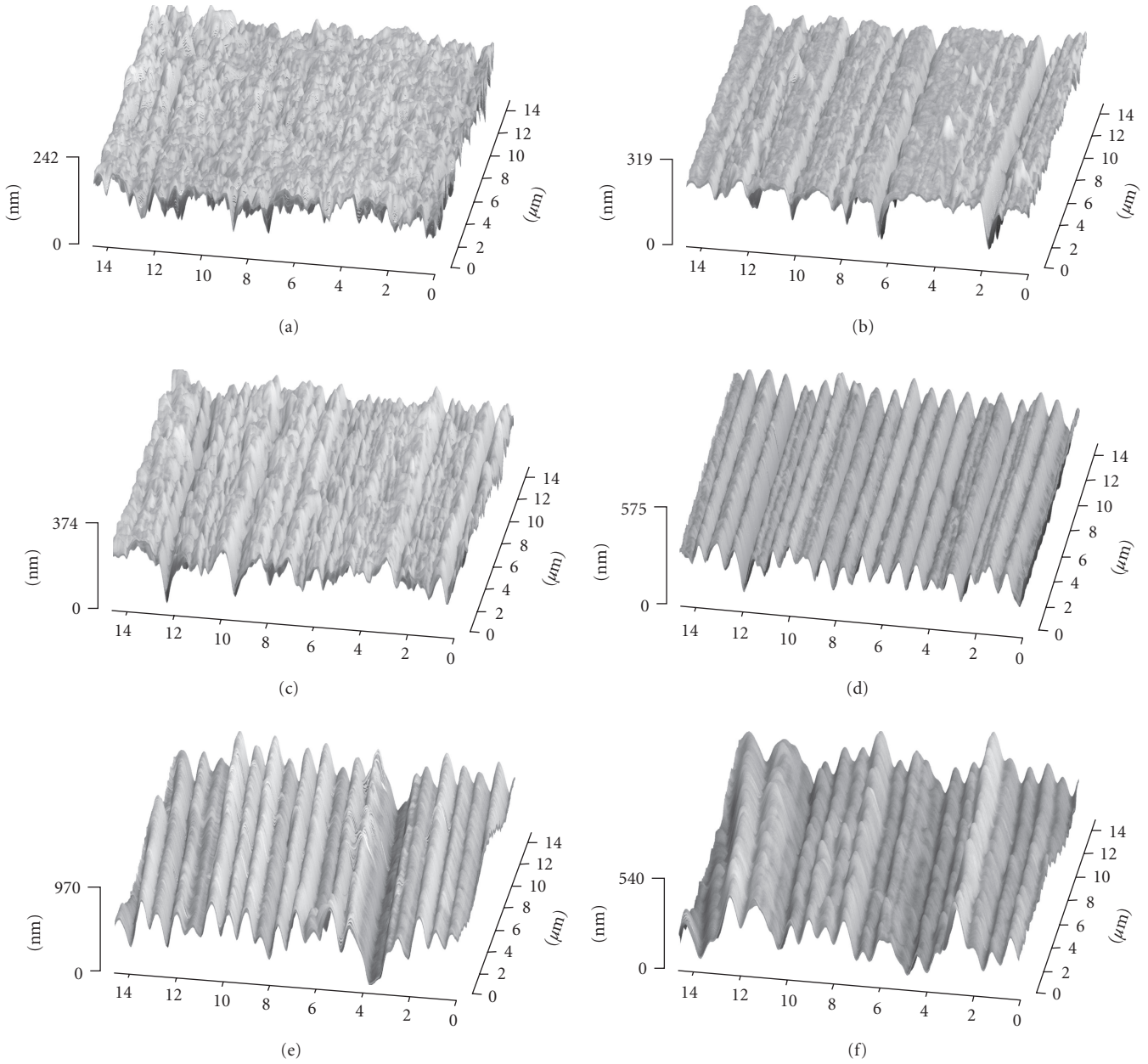

Figure 5: AFM surface plots of the banded surface morphology after (a) 5 s, (b) 10 s, (c) 20 s, (d) 40 s, (e) 80 s, and (f) 160 s immersion in 50% acetic acid 50% nitric acid etching solution.

10 seconds to 40 seconds the band spacing is constant at ~650 nm. The effective band spacing increases in the 80-second- and 160-second-etched samples, once the surface becomes over-etched.

Atoms in the intercrystalline region are in a nonequilibrium state and are generally expected to have lower corrosion resistance [19]. In conventional polycrystalline materials this can be seen as localized grain boundary attack. Grain size reduction to the nm-scale is expected to have a significant effect on the overall dissolution rate, largely because of the increased grain boundary and triple-line density intersecting the free surface [20, 21]. A study of the corrosion behavior of nanocrystalline and conventional polycrystalline Ni found a larger passivation current density for nanocrystalline compared to polycrystalline Ni [20]. X-ray photoelectron spectroscopy of the same samples polarized in the passive region showed a more defective passive layer for the nanocrystalline material [21]. The increased dissolution rate of nanocrystalline materials can also be seen from chemical machining studies of polycrystalline [22] and nanocrystalline Ni [23]; machining rates in nanocrystalline Ni were approximately an order of magnitude higher than conventional polycrystalline Ni for the same $FeCl_3$ aqueous solution concentrations [23].

In the present case, the characteristic grain boundary spacing is more than an order of magnitude finer than

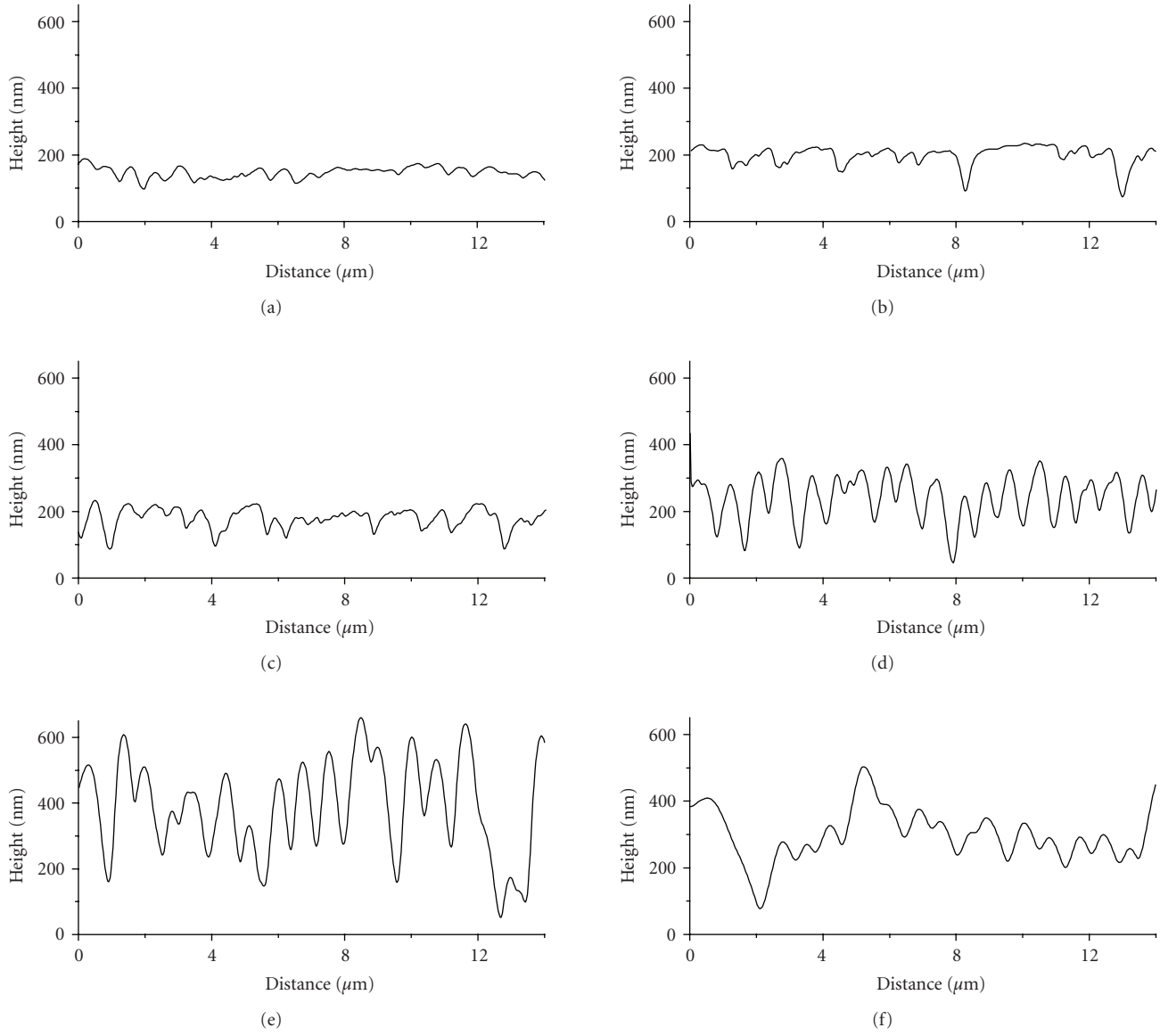

Figure 6: AFM profile plots after (a) 5 s, (b) 10 s, (c) 20 s, (d) 40 s, (e) 80 s, and (f) 160 s immersion in 50% acetic acid 50% nitric acid etching solution.

the sub-μm channel spacing. It should be noted that no significant change in grain size or grain-size distribution was seen across the compositional bands. Therefore, while grain-size reduction likely has a significant effect on the overall dissolution rate, it likely has comparatively little effect on the differential etching rate that forms the surface nanopattern. More significant are the Fe and Ni compositional variations in the through thickness direction; STEM/EDS line profiles across the compositional variations found that the relative intensity of the Fe signal ranged from ~30% to ~50% [13]. While it is known that the primary passivation potential of binary Ni-Fe alloys generally increase with increasing Ni concentration [24], comparatively little study has been conducted on the corrosion behavior of these alloys in nanocrystalline form. A study on the pitting behavior of nanocrystalline Ni-18%Fe found that it was more susceptible to pitting corrosion after significant grain growth had occurred during annealing [25]. Another study comparing the corrosion resistance of electrodeposited nanocrystalline Ni-W and Ni-Fe-W alloys reported poor corrosion resistance for the ternary alloy because of preferential dissolution of Fe [26]. While alloy concentration effects on the corrosion rate of electrodeposited nanocrystalline Ni-Fe alloys remain to be clearly established, the differential etching seen in the present study may be related to the preferential corrosion of compositional bands having higher Fe concentrations.

The evolving surface morphology can also be quantified in terms of surface roughness parameters. Figure 8 presents the average roughness, R_a , and the root-mean-square roughness, R_{RMS} , measured perpendicular to the band orientation as a function of etching time. Both roughness parameters (Figure 8) followed a similar trend to that of the band height

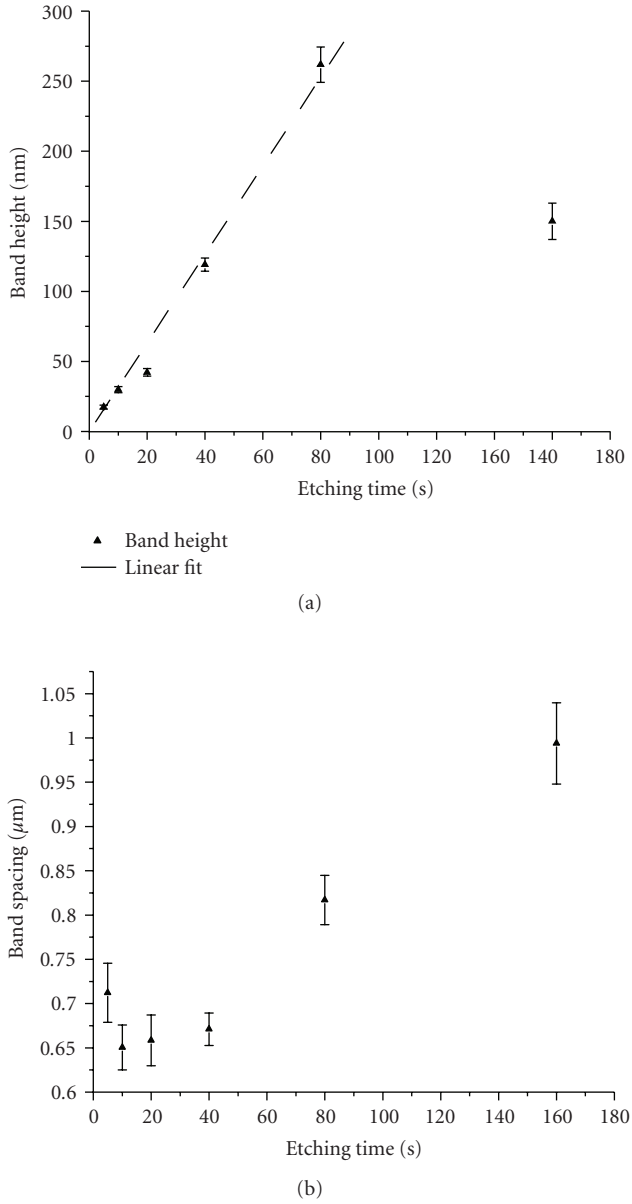

Figure 7: Mean band height (a) and band spacing (b) as a function of etching time in a solution of 50% acetic acid and 50% nitric acid. Error bars indicate the standard error in the mean.

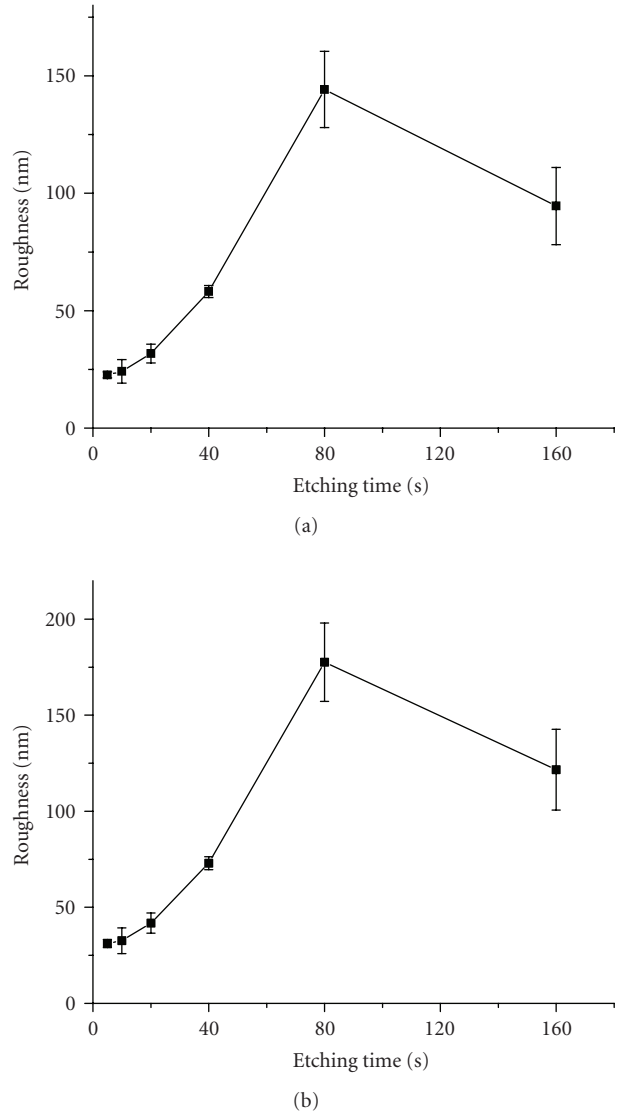

Figure 8: Evolution of the average roughness (a) and RMS roughness (b) with increasing etching time. Error bars give the standard error in the mean.

(Figure 7(a)) as a function of etching time. One measure of the band straightness is given by the angular distribution in surface roughness. Line profile average roughness values R_a and R_{RMS} were obtained in 10° increments from 0° (parallel to the bands) to 90° (perpendicular to the bands) and are presented as a series of polar plots in Figure 9. In each case, the surface roughness perpendicular to the bands is ~6 times greater than the surface roughness parallel to the bands. For example, after 40 seconds of etching time the R_a value is 62±7.6 nm perpendicular to the bands and 11±4.4 nm parallel to the bands. In fact the average roughness is nearly constant at ~60 nm over the angular range of 10° to 90°; it is only when the surface roughness is measured nearly parallel to the bands that it decreases significantly.

In addition to surface modification by varying the etching conditions, it is possible to manipulate the mesoscale compositional modulations themselves during electrodeposition. Self-assembled compositional modulations in conventional electrodeposits can be manipulated through synthesis parameters such as temperature, duty cycle, and plating current [27]. Periodic adjustments to these parameters during deposition of nanocrystalline electrodeposits could be used to modify the compositional modulations and provide a mechanism for controlling the resultant band structure. In addition, the overall compositional modulations are conformal to the cathode surface. This means that curved channels can be engineered by designing appropriate cathode geometries.

The ability to engineer the surface structure of nanocrystalline Ni-Fe alloys may add new functionalities to nanocrystalline electrodeposits in micro and nanoscale applications.

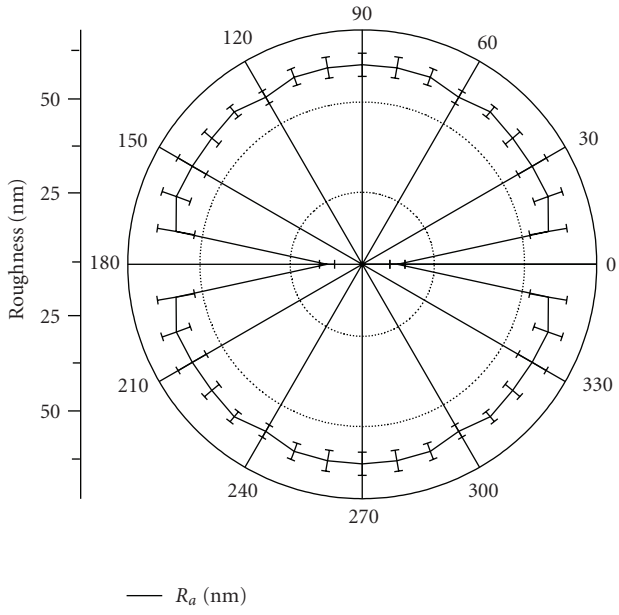

(a)

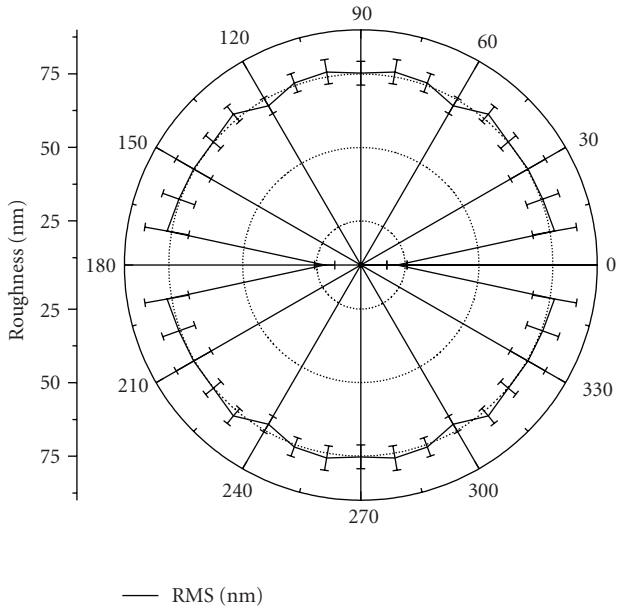

(b)

Figure 9: Polar plots giving the average roughness (a) and RMS roughness (b) as a function of angle measured with respect to the band orientation (0° is parallel to bands). Error bars give the standard error in the mean.

Conventional Ni alloy electrodeposits have become increasingly important components in MEMS devices [e.g., [28]], and reducing the grain size of these deposits to the nanocrystalline regime may significantly improve their performance [12]. Nanocrystalline electrodeposits have substantially increased strength, hardness, and wear resistance compared to conventional polycrystalline electrodeposits [e.g., [29]]. For example, more than a factor of three increase in yield strength is often observed, which can correspond to an approximately ten fold increase in the elastic energy storage capacity [29]. Furthermore, nanostructured electrodeposits offer increased uniformity in elastic properties when device components are scaled to the microscale regime and below [12]. Finally, the surface roughness directionality illustrated in the present study may provide new opportunities for controlling the relative movement of micro and nanoscale components by frictional forces.

4. CONCLUSIONS

Selective dissolution of nanocrystalline Ni-Fe electrodeposits was used to create periodic and regular nanopatterned surfaces. TEM characterization showed an ultrafine and uniform nanocrystalline grain size. Self-assembled alloy and impurity compositional modulations in the electrodeposit resulted in preferential etching of recessed channels that were aligned perpendicular to the growth direction and were continuous along the cross-section. AFM was used to characterize the nanopatterned surfaces; before over-etching, there was an initial linear differential etching rate between peak height and valley depth. The surface morphology was also quantified in terms of roughness parameters and their angular distribution. The surface roughness was approximately constant over an angular range from 10° to 90° inclination to the channels and nearly six times greater than parallel to the channels. Engineering the surface structure of Ni-Fe alloy electrodeposits may add new functionalities to nanocrystalline materials in micro and nanoscale applications.

ACKNOWLEDGMENTS

Financial support for this research was provided by the Natural Science and Engineering Research Council (NSERC). P. Egberts was supported by University of Toronto Open Fellowship.

REFERENCES

[1] R. C. Newman, S. G. Corcoran, J. Erlebacher, M. J. Aziz, and K. Sieradzki, "Alloy corrosion," *MRS Bulletin*, vol. 24, no. 7, pp. 24–28, 1999.

[2] N. A. Senior and R. C. Newman, "Synthesis of tough nanoporous metals by controlled electrolytic dealloying," *Nanotechnology*, vol. 17, no. 9, pp. 2311–2316, 2006.

[3] A. W. Hassel, B. B. Rodriguez, S. Milenkovic, and A. Schneider, "Fabrication of rhenium nanowires by selective etching of eutectic alloys," *Electrochimica Acta*, vol. 51, no. 5, pp. 795–801, 2005.

[4] J. Rösler and D. Mukherji, "Design of nanoporous superalloy membranes for functional applications," *Advanced Engineering Materials*, vol. 5, no. 12, pp. 916–918, 2003.

[5] D. Mukherji, G. Pigozzi, F. Schmitz, O. Näth, J. Rösler, and G. Kostorz, "Nano-structured materials produced from simple metallic alloys by phase separation," *Nanotechnology*, vol. 16, no. 10, pp. 2176–2187, 2005.

[6] S. D. Leith and D. T. Schwartz, "*In-situ* fabrication of sacrificial layers in electrodeposited NiFe microstructures," *Journal of Micromechanics and Microengineering*, vol. 9, no. 1, pp. 97–104, 1999.

[7] S. Arai, T. Hasegawa, and N. Kaneko, "Fabrication of 3-D Ni/Cu multilayered microstructure by selective etching of Ni," *Journal of the Electrochemical Society*, vol. 150, no. 11, pp. C798–C801, 2003.

[8] C.-Y. Lim, Q. Huang, X. Xie, et al., "Development of an electrodeposited nanomold from compositionally modulated alloys," *Journal of Applied Electrochemistry*, vol. 34, no. 8, pp. 857–866, 2004.

[9] Q. Huang and E. J. Podlaha, "Selective etching of CoFeNiCu/Cu multilayers," *Journal of Applied Electrochemistry*, vol. 35, no. 11, pp. 1127–1132, 2005.

[10] N. Wang, Z. Wang, K. T. Aust, and U. Erb, "Isokinetic analysis of nanocrystalline nickel electrodeposits upon annealing," *Acta Materialia*, vol. 45, no. 4, pp. 1655–1669, 1997.

[11] J. L. McCrea, G. Palumbo, G. D. Hibbard, and U. Erb, "Properties and applications for electrodeposited nanocrystalline Fe-Ni alloys," *Reviews on Advanced Materials Science*, vol. 5, no. 3, pp. 252–258, 2003.

[12] M. Baghbanan, U. Erb, and G. Palumbo, "Nanostructured Metals for Enhanced Performance of LIGA Components," in *Surfaces and Interfaces in Nanostructured Materials and Trends in LIGA, Miniaturization and Nanoscale Materials*, S. M. Mukhopadhyay, S. Seal, N. Dahotre, A. Agarwal, J. E. Smugeresky, and N. Moody, Eds., pp. 307–315, TMS, Warrendale, Pa, USA, 2004.

[13] P. Egberts, P. Brodersen, and G. D. Hibbard, "Mesoscale structure in electrodeposited nanocrystalline Ni-Fe alloys," *Materials Science and Engineering A*, vol. 441, no. 1-2, pp. 336–341, 2006.

[14] U. Erb and A. M. El-Sherik, "Nanocrystalline metals and process of producing the same," US patent 5,352,266, October 1994.

[15] U. Erb, A. M. El-Sherik, C. K. S. Cheung, and M. J. Aus, "Nanocrystalline metals," US patent 5,433,797, July 1995.

[16] C. Cheung, F. Djuanda, U. Erb, and G. Palumbo, "Electrodeposition of nanocrystalline Ni-Fe alloys," *Nanostructured Materials*, vol. 5, no. 5, pp. 513–523, 1995.

[17] F. Czerwinski, H. Li, M. Megret, J. A. Szpunar, D. G. Clark, and U. Erb, "The evolution of texture and grain size during annealing of nanocrystalline Ni-45% Fe electrodeposits," *Scripta Materialia*, vol. 37, no. 12, pp. 1967–1972, 1997.

[18] H. Q. Li and F. Ebrahimi, "An investigation of thermal stability and microhardness of electrodeposited nanocrystalline nickel-21% iron alloys," *Acta Materialia*, vol. 51, no. 13, pp. 3905–3913, 2003.

[19] D. A. Jones, *Principles and Prevention of Corrosion*, Prentice-Hall, Upper Saddle River, NJ, USA, 2nd edition, 1996.

[20] R. Rofagha, R. Langer, A. M. El-Sherik, U. Erb, G. Palumbo, and K. T. Aust, "Comparison of the Corrosion Behaviour of Nanocrystalline and Normal Crystalline Nickel," *Material Research Society Symposium Proceedings*, vol. 238, pp. 751–755, 1992.

[21] R. Rofagha, U. Erb, D. Ostrander, G. Palumbo, and K. T. Aust, "The effects of grain size and phosphorus on the corrosion of nanocrystalline Ni-P alloys," *Nanostructured Materials*, vol. 2, no. 1, pp. 1–10, 1993.

[22] C. Y. Liao and J. K. Wu, "Chemical machining of nickel in ferric chloride solution," *Journal of Materials Science Letters*, vol. 11, no. 10, pp. 689–691, 1992.

[23] S. Ho, T. Nakahara, and G. D. Hibbard, "Chemical machining of nanocrystalline Ni," *Journal of Materials Processing Technology*. In press.

[24] F. Berthier and F. Priester, "Electrochemical properties," in *The Iron-Nickel Alloys*, G. Beranger, F. Duffaut, J. Morlet, and J. F. Tiers, Eds., pp. 241–263, Lavoisier, Paris, France, 1996.

[25] R. V. Steward, G. J. Fan, L. F. Fu, et al., "Pitting behavior of a bulk Ni-18 wt.% Fe nanocrystalline alloy," *Corrosion Science*, vol. 50, no. 4, pp. 946–953, 2008.

[26] K. R. Sriraman, S. Ganesh Sundara Raman, and S. K. Seshadri, "Corrosion behaviour of electrodeposited nanocrystalline Ni-W and Ni-Fe-W alloys," *Materials Science and Engineering A*, vol. 460-461, pp. 39–45, 2007.

[27] C. C. Nee and R. Weil, "The banded structure of Ni-P electrodeposits," *Surface Technology*, vol. 25, no. 1, pp. 7–15, 1985.

[28] S. M. Spearing, "Materials issues in microelectromechanical systems (MEMS)," *Acta Materialia*, vol. 48, no. 1, pp. 179–196, 2000.

[29] U. Erb, K. T. Aust, G. Palumbo, J. McCrea, and F. Gonzalez, "Electrodeposited Nanostructured Materials," in *Processing and Fabrication of Advanced Materials IX*, T. S. Srivatsan, R. A. Varin, and K. A. Kohr, Eds., pp. 253–262, ASM International, Materials Park, Ohio, USA, 2001.